SMR/543 - 20

EXPERIMENTAL WORKSHOP ON
HIGH TEMPERATURE SUPERCONDUCTORS AND RELATED MATERIALS
(BASIC ACTIVITIES)

(11 February - 1 March 1991)

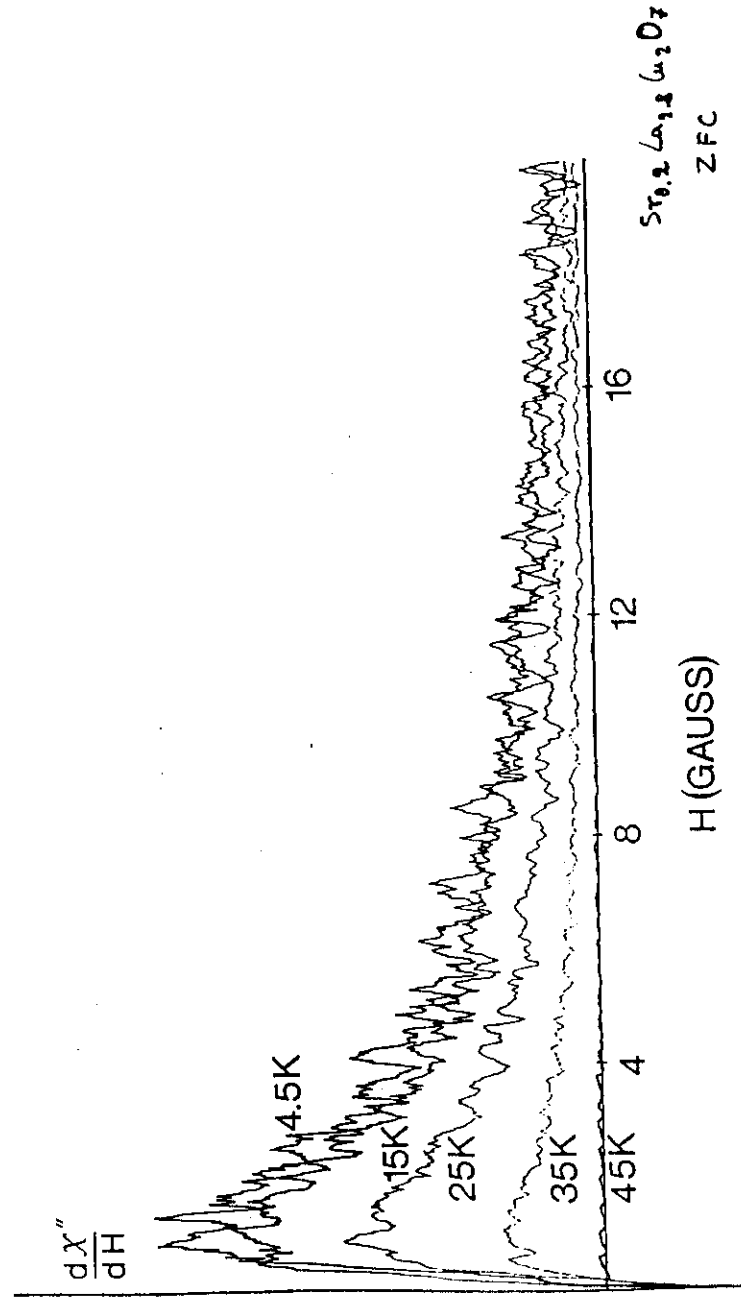" EPR Spectroscopy and Microwave Absorption of HTS Materials "

PART II

presented by:

G. AMORETTI
Università degli Studi di Parma
Dipartimento di Fisica
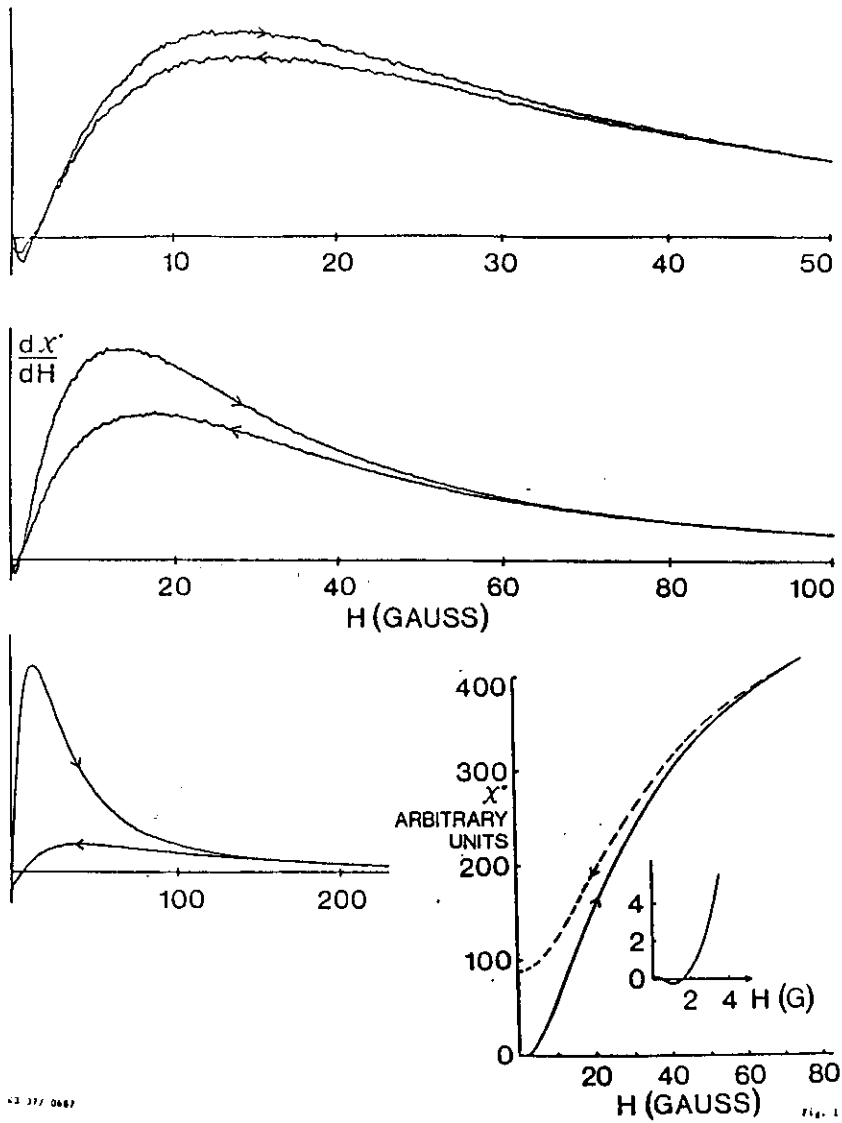Viale delle Scienze
43100 Parma
Italy

The main features of the superconductive absorption are:

1) fluctuating character, more evident at low field;

2) reproducibility of some of the fluctuations by varying the field;

3) hysteretic irreversibility strongly dependent on both the extreme field of the sweep and the modulation intensity;

4) different behaviour in the case of zero-field-cooling (ZFC) and non-zero-field-cooling (FC), with magnetic memory effects;

5) position of the maximum strongly sample dependent. Usually in the 0.1-20 Oe range for ZFC samples (values up to 100 Oe have been observed);

6) temperature dependence of field and height of the peak, the last one being very strong.
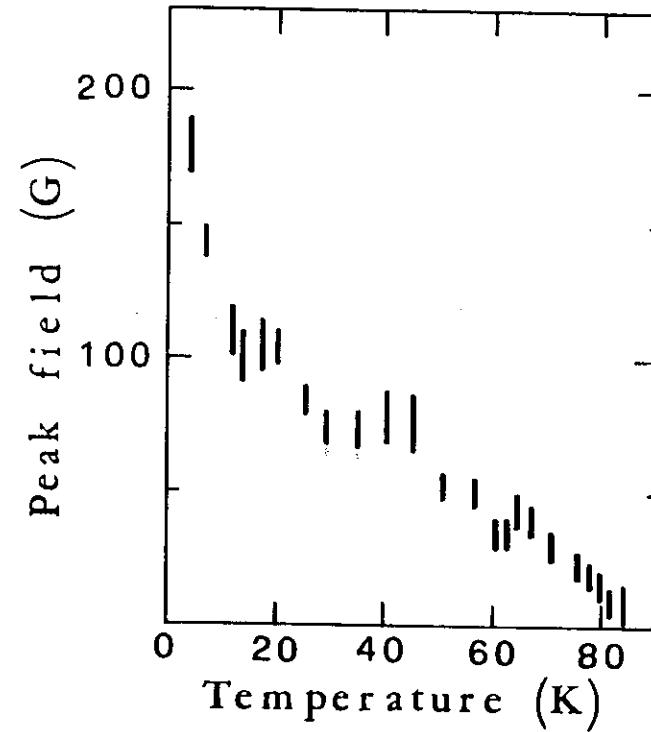

$Sr_{0.2} La_{1.8} Cu_2 O_7$

ZFC

$\frac{dX''}{dH}$

4.5K
15K
25K
35K
45K

H (GAUSS)

4 8 12 16

Blazey, K.A. Müller, J. G. Bednorz, W. Berlinger, E. Baluggiu, A. Vera and F. C. Matacotta, Phys. Rev. B 36 (1987) 7241

$\frac{d\mathcal{X}'}{dH}$

H (GAUSS)

$\mathcal{X}'$ ARBITRARY UNITS

400
300
200
100
0

4
2
0
2 4 H (G)

20 40 60 80
H (GAUSS)

200

Peak field (G)

100

0   20   40   60   80
Temperature (K)
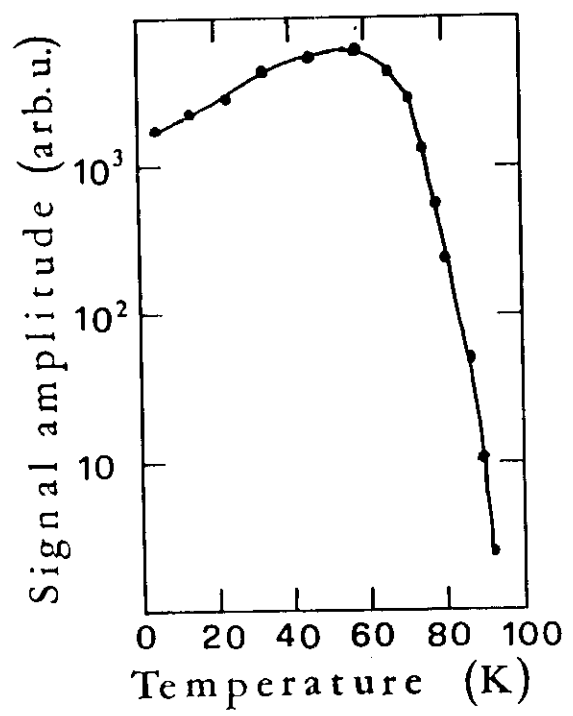
E. Buluggiu, G. Amoretti and A. Vera,
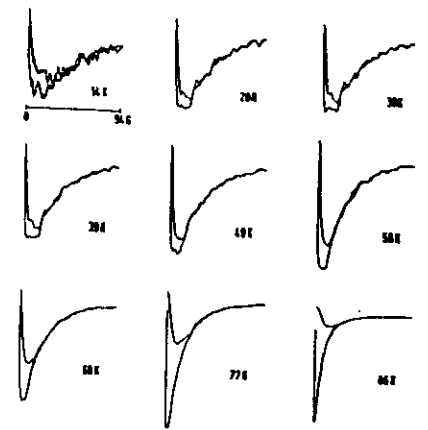Vuoto: Scienza e Tecnologia XVIII, 288 (1988).

Fig. 1. Temperature dependence of the field-modulated microwave absorption of ZFC samples for a fixed field scan of 0–94–0 G. The back trace always results in a smaller variation of the signal. The received gain was kept constant from 14–58 K, and then reduced to 80% for the signals at 68 and 77 K, and to 63% at 86 K. The field modulation amplitude was 5 G (peak-to-peak).
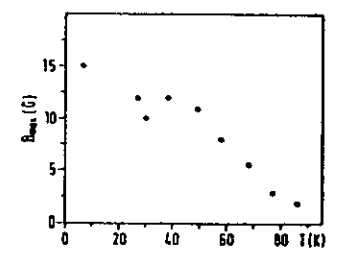

Fig. 2. Temperature dependence of the maximum of the field-modulated microwave absorption for the increasing field scan using a zero-field cooled sample.

for the particular field scan of 94 G. The position of the broad maximum also shows a temperature dependence, which is depicted in fig. 2. A similar, although much larger variation of the peak positions was already reported [6,7] for the same material. The similarity of the values quoted in ref. [6] with the independently determined lower critical field H_{c1} [8] was taken as evidence that the peak position of the

$d\chi''(B)/dB$-trace can be used to determine H_{c1} in a simple fashion.

Quite contrary we think that the only indicator for H_{c1} is the observation of hysteresis in the $d\chi''(B)/dB$-curve, because flux penetration into the bulk superconductor is expected only for field values above H_{c1}, with a subsequent modification of the superconducting network, whose phase slipping is documented via the fine structure of the microwave absorption.

In order to exclude a slow time dependence in the flux penetration, the field scan was stopped at the highest field value for approximately 1 h. The resulting backtrace was indistinguishable from the prompt sweep, thus excluding time-dependent effects on the one-hour time scale.

Our hypothesis was further tested by determining the minimum field sweep range ΔB, for which noticable hysteresis could be observed as a function of the temperature. The result is plotted in fig. 3. Here hysteresis $H(T, \Delta B)$ is defined by the ratio of the differences in peak amplitudes for the increasing and decreasing field scans, respectively, and the peak amplitude ΔB for the increasing field scan. Deliberately, we determined $H_{c1} = \Delta B$ for a value of $H(T, \Delta B) = 30\%$. The observed qualitative agreement of $H_{c1} = f(T)$ with a simple $H_{c1}(T) = H_{c1}(0)(1 - (T/$
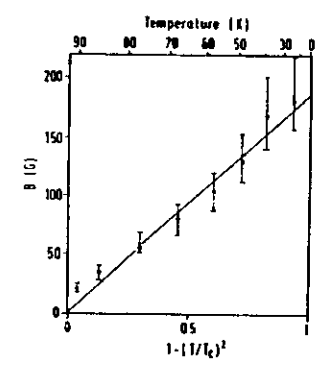

Fig. 3. Temperature dependence of the critical field H_{c1} as deduced from the hysteresis onset of the microwave absorption scans. The error bars were obtained by evaluating the $H_{c1}(T)$ dependence for hysteresis onsets of 20 and 40%, respectively. For the normalized plot we used $T_c = 92.1$ K.

E. Buluggiu, G. Amoretti and A. Vera,
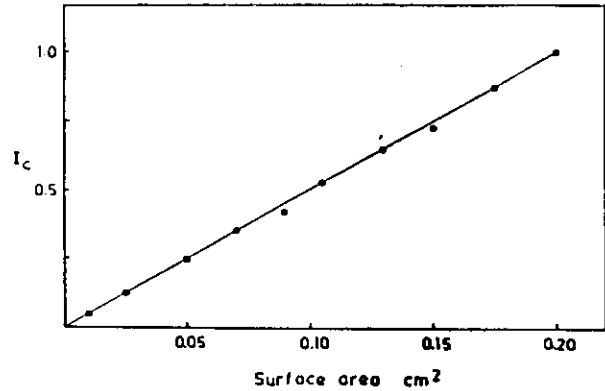Varto : Scienza e Tecnologia XVIII , 28? (1988)

Fig. 13. The intensity of the microwave signal such as that of fig. 8, as a function of surface of the plate like sample chips.
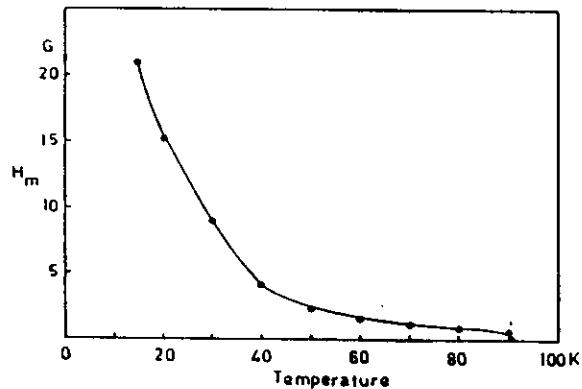

Fig. 14. Shift of the centre of the signal of fig. 8 upon cooling.

The signal is associated to the fluxon dynamic within the granular structure of the compound.

In the framework of the *superconducting glass* model, the field position of the absorption peak in a ZFC sweep allows us to estimate the average dimension of the single region of uniform phase.

If we assume that this field is associated with the critical field H_{c1}^* where flux slips start to occur, the average projected area of the superconducting loops in the glassy state is given by:

$$S = \phi_0/2H_{c1}^*,$$

where $\phi_0 = 2.07 \cdot 10^{-7} G \cdot cm^2$ is the elementary flux quantum.

$$\mathcal{H} = -\sum_{ij} J_{ij} \cos(\phi_i - \phi_j - A_{ij}) \ .$$

The phase factors $A_{ij} = \kappa_{ij}H$ introduce randomness and frustration in the presence of a magnetic field H because the system has many competing ground states of almost the same energy. κ_{ij} is a random geometric factor. Hence, after cooling in zero magnetic field the system is in a Meissner or XY state.[3-5] On the application of a magnetic field, the system is weakly random and changes its configuration with accompanying flux slips starting at a critical field H_{c1}^*.

TABLE I. Variation of H_{c1}^* in the different superconducting copper oxides used in the low-field microwave absorption experiments.

	H_{c1}^* (gauss)	Cluster radius mμ	T_c (K)
$Ba_{0.15}La_{1.85}CuO_4$	13.5	0.7	26
$Sr_{0.2}La_{2.8}Cu_2O_7$	0.8	2	35
$Sr_{0.2}La_{1.8}CuO_4$	0.6	2.3	40
$Y_{1.8}Ba_{1.2}Cu_3O_{7-\delta}$	0.5	2.5	90
$YBa_2Cu_3O_{7-\delta}$	~3-20	1.0-0.4	92
$YBa_3Cu_4O_{9-\delta}$	~8	0.6	92

K.W. Blazey, K.A. Müller, J.G. Bednorz, W. Berlinger, G. Amoretti, E. Buluggiu, A. Vera and F.C. Matacotta, Phys. Rev. B **36**, 7241 (1987).

In the framework of the Josephson junctions coupling mechanism in a granular medium, the effective junction length can be estimated from

$$d \sim \phi_0/(2H_{max}\lambda_L),$$

H_{max} being the field at the derivative absorption maximum, roughly corresponding to the half-width of an average Fraunhofer-like diffraction pattern for the screening supercurrents through the array of differently sized junctions.

Typically, with $\lambda_L = 500\text{Å}$, a field of 10 G will produce a quantum flux through a junction when $d = 20\mu m$.
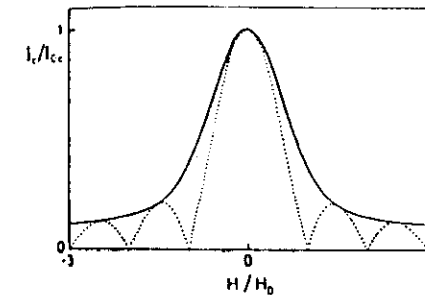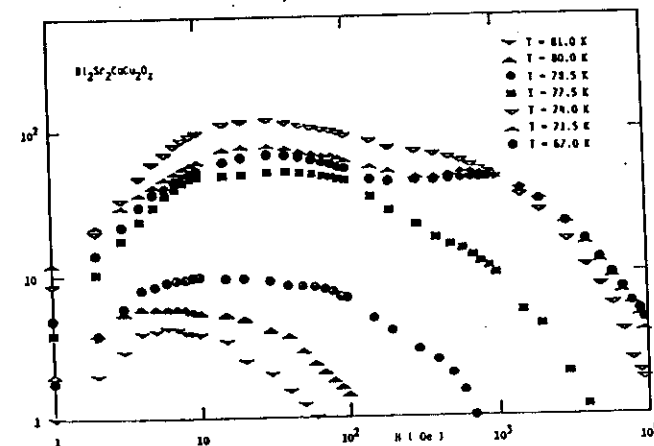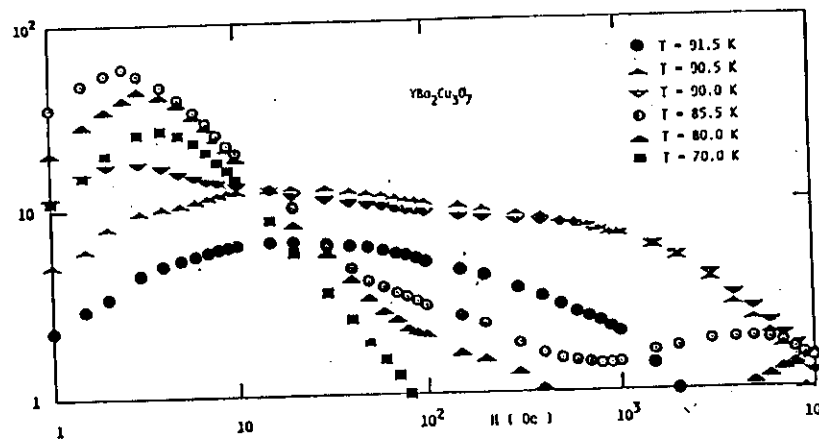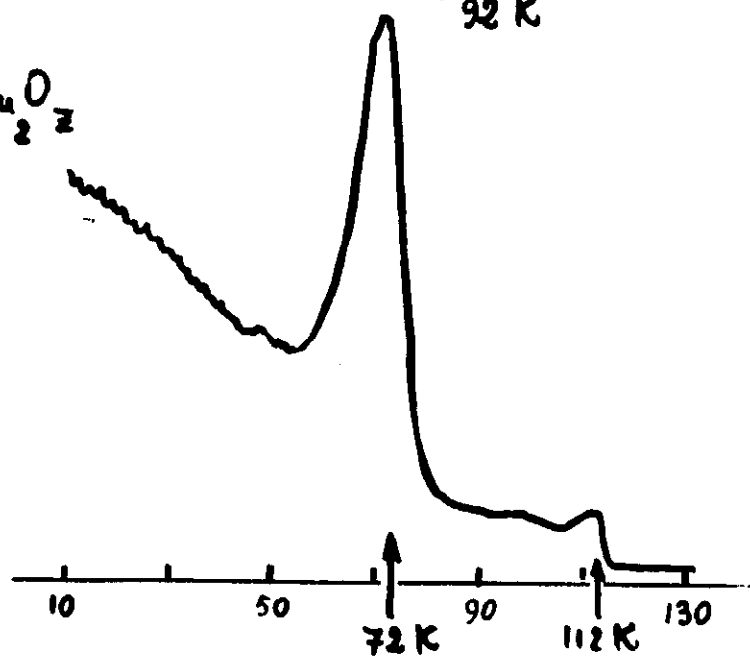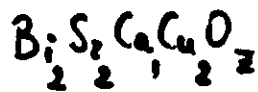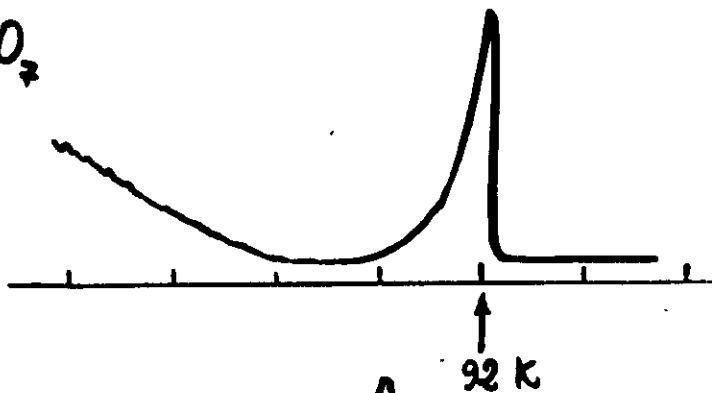
It seems by now well established that in the ceramic supercon-

ducting oxides the H-modulated non-resonant microwave absorption

signal, as detected below T_c by a conventional ESR spectrometer,

comes out essentially from two distinct contributions:

- one of them, drastically dependent on preparation, annealing

  and (in powdered samples) grain size, is predominant in the

  low-field and low-temperature region. It is generally very intense

  and probably related to *viscous flux motion* or to *phase slippage*

  processes in the intergrain network of Josephson junctions;

- the other, observed in a more restricted temperature range near

  T_c and almost independent of the preparation details, appears to

  be strictly related to the *resistivity drop* and then to intragrain

  effects. It is comparatively weaker and reaches its maximum

  intensity in a moderate field ($H \sim 50\ Oe$).

Magnetic Field (G)
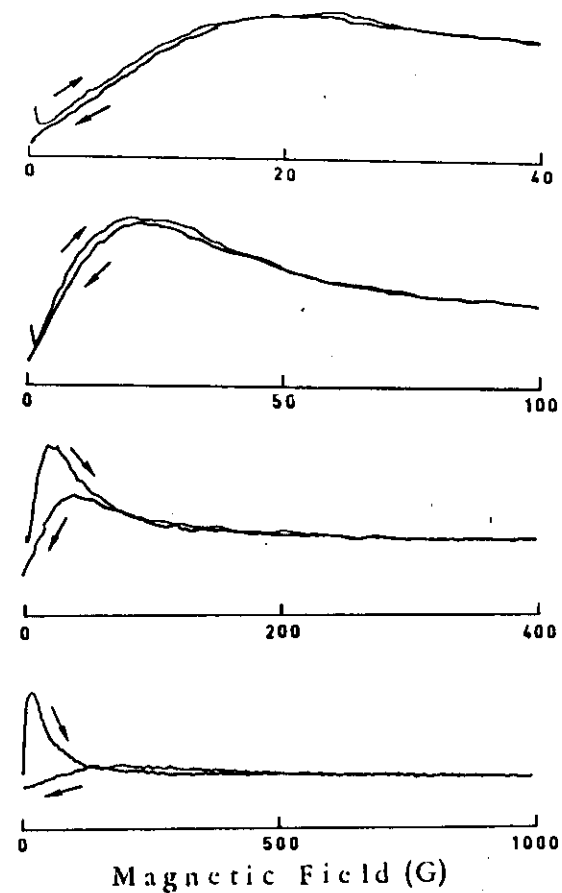
E. Buluggiu, G. Amoretti and A. Vera,
Vuoto: Scienza e Tecnologia XVIII, N.3, 288 (1988)

$Y Ba_2Cu_3O_7$

$Bi_2S_2Ca_1Cu_2O_7$

92 K

72 K   112 K

10   50   90   130

$YBa_2Cu_3O_7$

- T = 91.5 K
- T = 90.5 K
- T = 90.0 K
- T = 85.5 K
- T = 80.0 K
- T = 70.0 K

H (Oe)

$Bi_2Sr_2CaCu_2O_2$

- T = 81.0 K
- T = 80.0 K
- T = 78.5 K
- T = 77.5 K
- T = 74.0 K
- T = 73.5 K
- T = 67.0 K

H (Oe)

E. Buluggiu and A. Vera , LT-19 Sat. Conf., Cambridge 1990

E. Buluggiu A. Vera D.C. Gioni G. Amoretti and F. Licci , SATT4 , Parma 199

derivative absorption (arb. un.)

2 G   3 G   7 G   12 G

30 G   45 G   100 G   500 G

1000 G   2000 G   5000 G   9500 G

T (K)
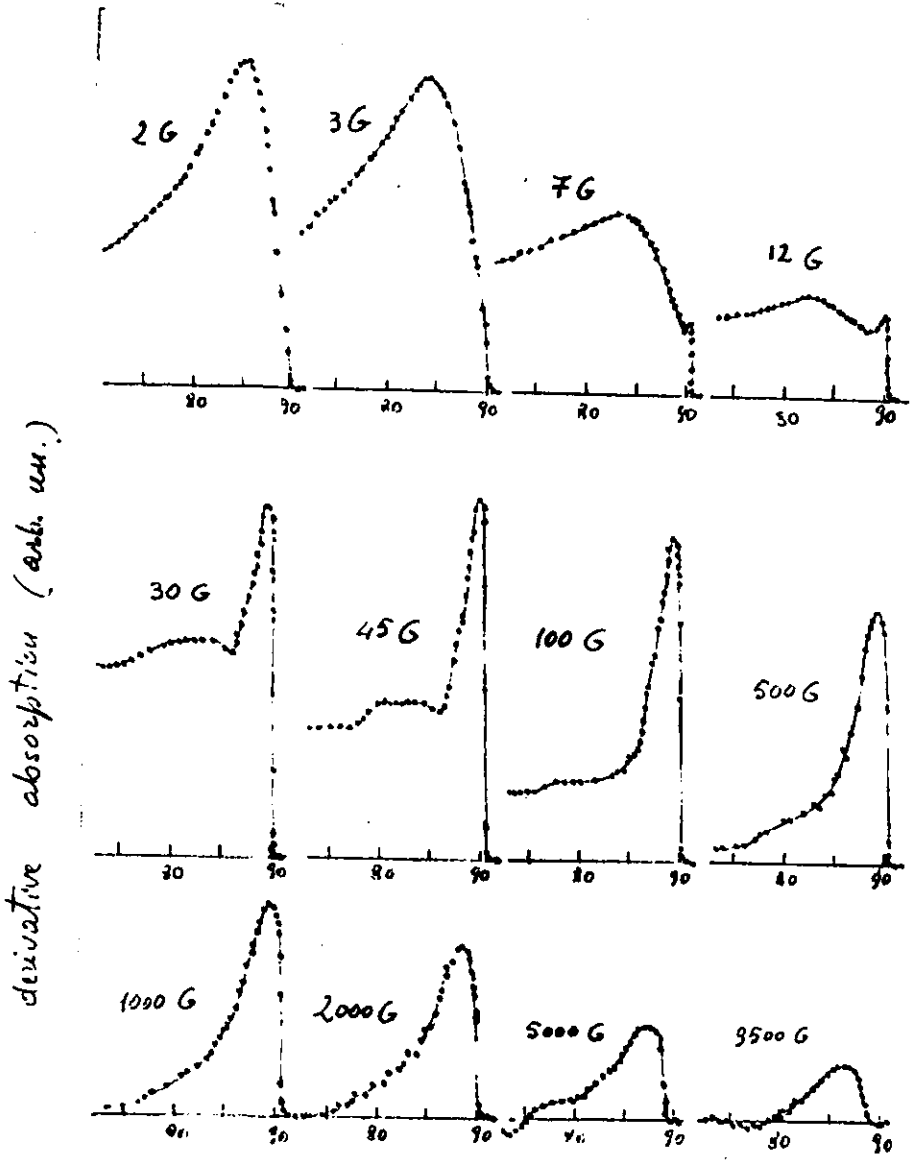
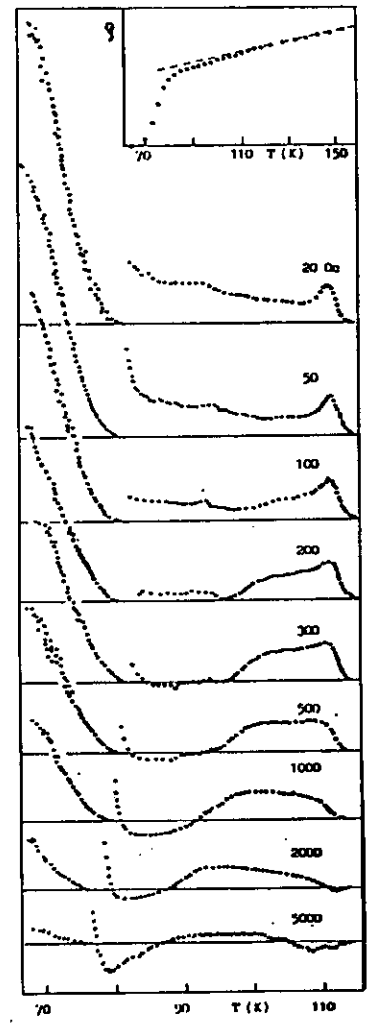E. Buluggiu, D.C. Giori, A. Valenti, A. Vera and

FIGURE 1
X-band microwave derivative absorption (arb.
units) vs temperature at different fields (Oe).
The gain in the low temperature part is 1/100.

20 Oe
50
100
200
300
500
1000
2000
5000

70   90   T (K)   110

E. Buluggiu, D.C. Giori, A. Valenti, A. Vera,

An ESR spectrometer measures the change in reflection coefficient of the microwave cavity, due to energy absorption, which is proportional to the surface resistivity of a superconducting sample.

Dissipation in superconductors due to viscous flux motions driven by the induced microwave currents is characterized by an effective surface impedance

$$Z = R - iX = -iX_0(1 + 2iB/B_0)^{1/2},$$

where

$$X_0 = 4\pi\omega\lambda_{eff}/c^2,$$

and

$$B_0 = 8\pi\omega\lambda_{eff}^2\eta/\phi_0.$$

In an increasing magnetic field fluxons first enter the weak links or Josephson junctions of a granular superconductor and then the bulk material only when the field exceeds H_{c1}.

The dominant absorption we observe is due to fluxons in the Josephson junctions. In fact, the microwave absorption (MWA) is inversely proportional to the viscosity, which has been estimated to be six order of magnitude lower in the junctions than in the bulk.

This can be seen easily without using modulation techniques: a change in slope in the absorption is observed when fluxons start entering the bulk, where they contribute less, taking into account also that they are sampled by the microwaves a skin depth in from the surface.

MWA can also arise from resistive losses in the normal cores of flux vortices in the mixed state, or from dissipation due to Josephson junction resistance in low fields.

It is then not surprising that hysteretic phenomena are present, related to trapped flux. In particular, when the external field is removed, the microwave absorption decreases, but not to its zero-field starting value: there is a remanent absorption, which is due to the remanent magnetization of the sample.
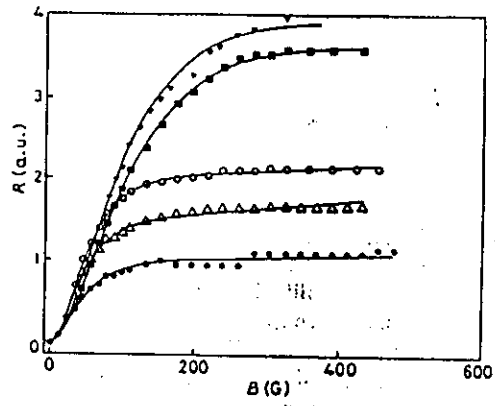
Fig. 4. – Single marks refer to measurements of the reflected power R of the cavity as a function of the external magnetic field B for different temperatures $T < T_c$. ▼ 23.0 K, ■ 34.5 K, ○ 70.5 K, △ 76.0 K, ● 83.5 K. Continuous lines show the best fit of the data obtained by using eq. (1) and an adjustable parameter B^*.

R. Fastampa, M. Giura, R. Marcon and C. Matacotta,
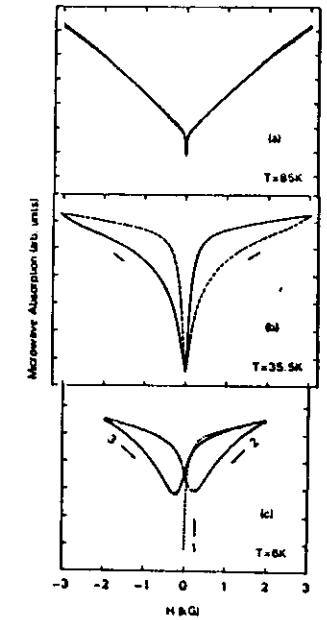Europhys. Lett. $\underline{6}$ (1988) 265

FIG. 1. Microwave absorption of granular Y-Ba-Cu-O vs applied dc magnetic field. (a) $T = 85$ K. Solid curve $dH/dt > 0$ and dashed curve $dH/dt < 0$ coincide. (b) $T = 35.5$ K. Solid curve $dH/dt > 0$ and dashed curve $dH/dt < 0$ form hysteresis loop. (c) $T = 6$ K. Dotted curve, initial field application, $dH/dT > 0$. Dashed curve, $dH/dt < 0$, and solid curve, $dH/dt > 0$, form subsequent hysteresis loop exhibiting large remanent absorption at $H = 0$.
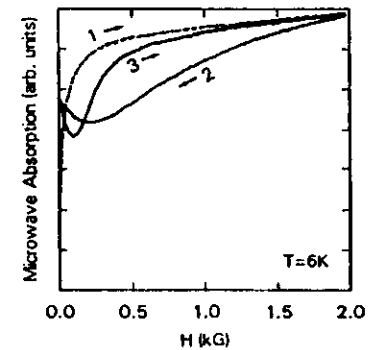

FIG. 2. Microwave absorption of granular Y-Ba-Cu-O vs applied magnetic field, $T = 6$ K. Dashed curve, initial field application. Solid curve, subsequent hysteresis loop, H positive.

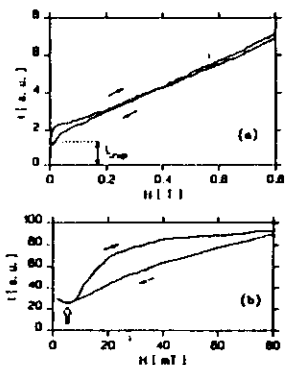E. J. Pakulis and T. Osada, Phys. Rev. B $\underline{37}$ (1988) 5940

Fig. 1. Direct microwave absorption signal in $Y_1Ba_2Cu_3O_7$ at 50 K. The sample was cooled in a magnetic field of 1.5 mT from 200 K to 50 K. Afterwards the field was swept between 1.5 mT and 0.8 T. (a) After one field cycle the absorption at the lowest field differs by I_{trap}. (b) Field dependence of microwave absorption after several field cycles. The double arrow indicates a small dip in absorption.
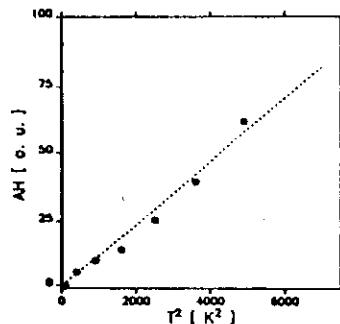

Fig. 2. The temperature dependence of the linear term in eq. (1). The quadratic temperature dependence arises from absorption within a vortex (see text).
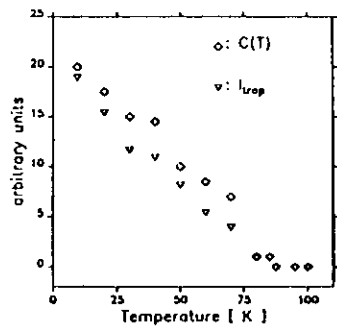

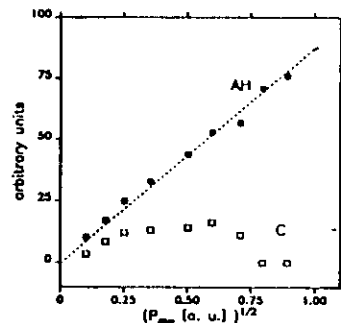Fig. 3. The temperature dependence of $C(T)$ in eq. (1) and I_{trap}.

Fig. 4. Microwave power (P_{mw}) dependence of the $A(T)H$ and $C(T)$ terms in eq. (1). The horizontal axis is proportional to the square root of the microwave power, i.e. proportional to the microwave field.

Another class of phenomena is connected with modulation effects. An ESR spectrometer measures normally the field derivative of the MWA by superimposing a small ac field parallel to the external one and detecting the absorption signal sincronously to this modulation field using lock-in techniques.

This is not always the case with superconducting samples, since MWA depends on their magnetization, which is not always reversible due to flux trapping even at low fields.

A prominent low-field hysteresis in signals recorded by means of field modulation was also observed, which was absent in curves recorded without modulation.

The MWA signal depends on the modulation amplitude and on the sign of the field sweep, but is insensitive to the modulation frequency and the rate of field sweep.

Y. Naniwa et al., Physica C156 (1988) 755

At small amplitudes, the signal changes sign with field reversal. As the modulation increases, the field-increasing and field decreasing curves came together from high fields, with the resulting curve an odd function of field.

This behaviour has its origin in the superconducting critical state that exists at the surface. Two processes contribute to the modulated absorption signal:

- one is due to the modulation of fluxon density and is independent of the direction of the external field sweep;

- the second is due to the surface critical current, changing sign sign with the field sweep.

In the limit of small modulation amplitudes and microwave field strength, the signal shapes are found to exhibit a peculiar evolution with the temperature, which can be interpreted in terms of *loss mechanism in intergranular Josephson junctions*.
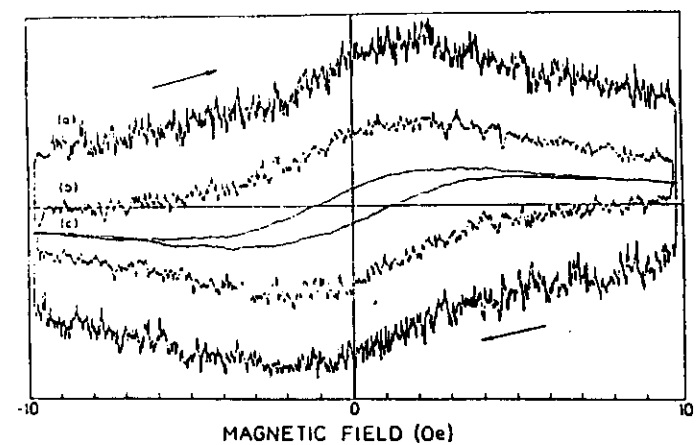

MAGNETIC FIELD (Oe)

Fig. 1. Microwave absorption signals of $YBa_2Cu_3O_{4.n}$ at 77 K in a field modulation and first harmonic lock-in detection scheme. (a) Peak-to-peak modulation amplitude (MA) 10 mOe, receiver gain (RG) 6.3×10^2, (b) MA 100 mOe, RG 6.3×10, (c) MA 1.Oe, RG 6.3. The microwave power was 10 mW.
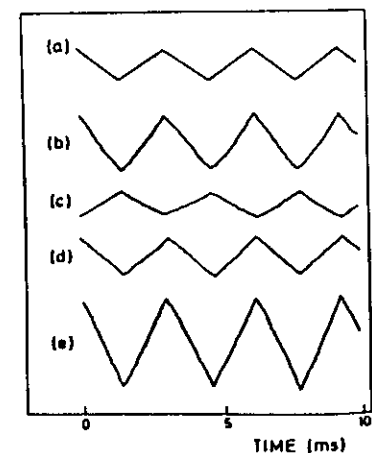

TIME (ms)

Fig. 2. (a) Magnetic field modulation, peak-to-peak 6 mOe, (b) and (c) variation of the microwave absorption in the up-field and down-field sweep respectively at 7 Oe, (d) and (e) curves deduced from the original signals in (b) and (c) by the procedure described in the text.
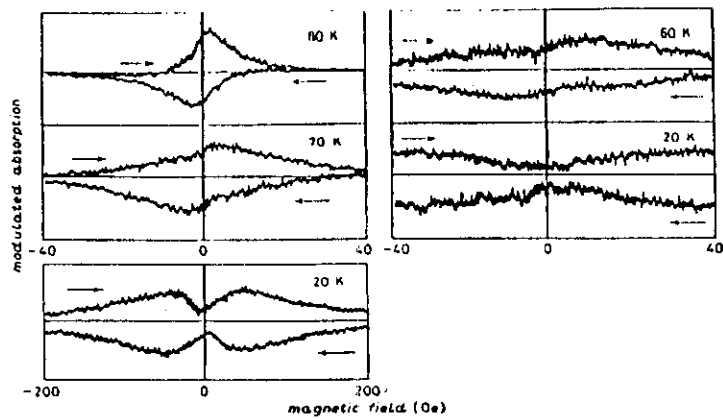
Fig. 1. – Modulated absorption of a ceramic superconductor $YBa_2Cu_3O_7$ at different temperatures. Microwave power was 1 mW and modulation amplitude 100 mOe.

$$\frac{Ch}{2e}\frac{d^2\phi}{dt^2} + \frac{1}{R}\frac{h}{2e}\frac{d\phi}{dt} + I_c \sin\phi = I_0 + I_{mw}\cos\omega_{mw}t + I_M \cos\omega_M t$$

$$P = P_n \frac{1}{1+\eta}$$

$$\eta = \frac{I_c^2 \cos^2\phi_0}{((1/R)(h/2e)\,\omega_{mw})^2}$$

$$S_M = \frac{((1/2)I_{mw}^2 R)^{1/2}}{((1/R)(h/2e)\,\omega_{mw})^2}\frac{I_c}{(1+\eta)^{3/2}}\left[-\frac{dI_c}{dH}H_M + I_M \sin\phi_0\right]\cos\omega_M t$$
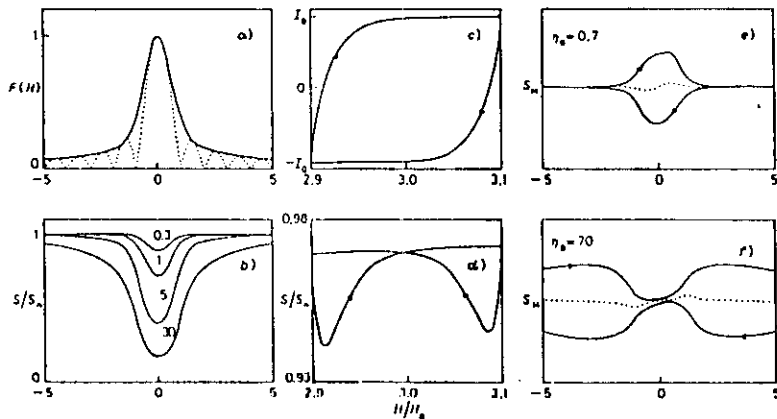
Fig. 2. – a) The diffraction pattern and its envelope $F(H)$ used as the reduction factor for the critical currents in Josephson junctions. b) Calculated microwave absorption signals for different values of η_0, indicated by the numbers. c) Model for the variation of the boundary current in a modulated magnetic field. d) Calculated variation of the microwave absorption with the modulation as in c). e) and f) Modulated absorption signals calculated for small modulation amplitudes ($H_M \ll H^*$) in forward and reverse field sweeps. Only $I_c^2(0, T) \sim \eta_0$ was changed in the calculations of the two spectra.

A. Dulčić et al., Europhys. Lett. 10, 593 (1989)

M. Požek et al., Physica C 169 (1990) 95

A. Dulčić, B. Rakvin and M. Požek,

Europhys Lett. 10. 593 (1989)

The phenomenon has also been explained by pinning and depinning of fluxons over a modulation field cycle.

A magnetic field applied to a granular superconductor (or a type II superconductor above H_{c1}) induces a critical state at the surface where the critical current is flowing already at very low fields. In this state all the depinned fluxons contribute to the microwave absorption.

Upon reversing the field sweep the critical current is reversed at the surface only after a certain field interval:

$$2H_{c1}' = (4\pi/c)\lambda' J_c \approx 2\pi\phi_0/\mu d^2,$$

where λ' is a flux relaxation distance.

For $d \approx 5\mu m$ we have $H_{c1}' \approx 5\ Oe$.

Within this interval, the current flowing at the surface is less than J_c, and some of the fluxons which were previously free become pinned and do not absorb microwaves.

This critical current modulation effect is dominating at small modulation amplitudes.

For temperatures well below T_c, the modulated absorption as a function of the modulation field H_m shows a minimum at $H_m \sim 2H_{c1}'$ indicating the passage to the regime in which the changing fluxon concentration signal prevails.

The temperature dependence of the two contribution to the modulated MWA signal is very different: the component due to the critical current modulation decreases linearly with increasing temperature, while that due to changing fluxon density is nearly constant over a wide temperature range and drops to zero around T_c.

K. W. Blazey et al., Solid State Commun. <u>65</u>, 1153 (1988)

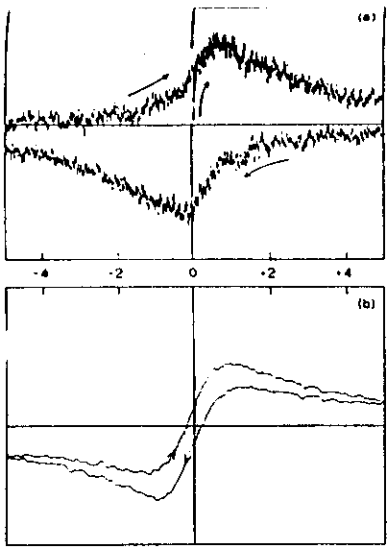K. W. Blazey and A. Höhler, Solid State Commun. <u>72</u> 1199 (1989)

Fig. 1. (a) Absorption signal at small modulation amplitudes. The signal changes sign with field reversal and is very similar to the magnetization measured. (b) Absorption signal at large modulation amplitudes. As the modulation increases, the field-increasing and field-decreasing curves came together from high fields with the resulting curve an odd function of field.
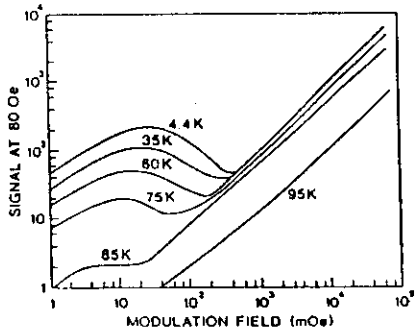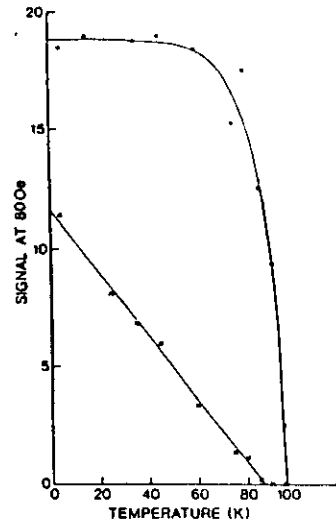

Fig. 3. Temperature dependence of the two contributions to the modulated microwave absorption of a ceramic $YBa_2Cu_3O_{7-\delta}$ sample. x: surface critical current component at 5 mOe modulation. •: fluxon density modulation at 2 Oe modulation.
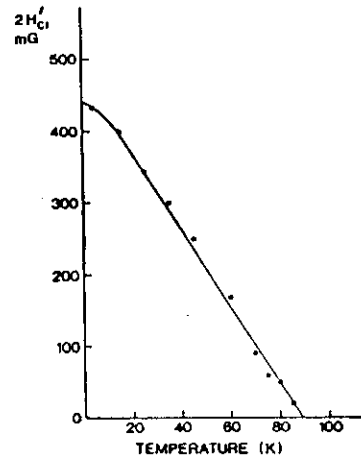

Fig. 4. Variation of the modulated microwave absorption signal at 80 Oe with the amplitude of the modulation field for different temperatures of the $YBa_2Cu_3O_{7-\delta}$ film used for Fig. 1.

$YBa_2Cu_3O_{7-\delta}$ THIN FILMS ON $LiNbO_3$

Fig. 5. Temperature dependence of the modulated microwave absorption of the $YBa_2Cu_3O_{7-\delta}$ film at • 100 mOe and x 5 Oe modulation field amplitudes.
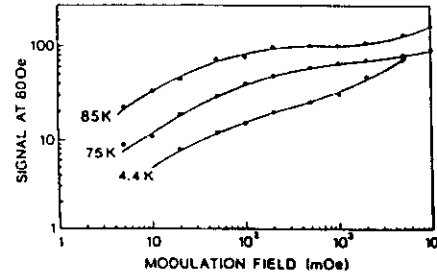

Fig. 2. Variation of the modulated microwave absorption signal at 80 Oe with the amplitude of the modulation field for different temperatures of a ceramic $YBa_2Cu_3O_{7-\delta}$ sample.

Fig. 4. Temperature variation of $2H'_{c1}$ for a $YBa_2Cu_3O_{7-\delta}$ taking the modulation field where the modulated microwave absorption goes through a minimum in Fig. 3.

Fig. 3. Temperature dependence of the modulated microwave absorption in arbitrary units at 80 Oe for a $YBa_2Cu_3O_{7-\delta}$ ceramic with a modulation amplitude of 5 mOe and a thin film with 100 mOe modulation amplitude.

K. W. Blazey, in "Earlier and Recent Aspects of Superconductivity",

K. W. Blazey and A. Höhler, Solid State Commun. 72, 1199 (1989)

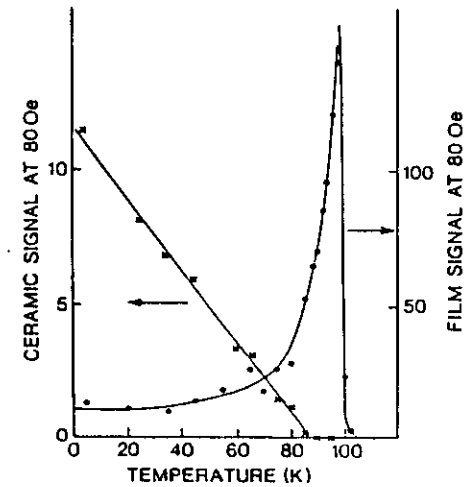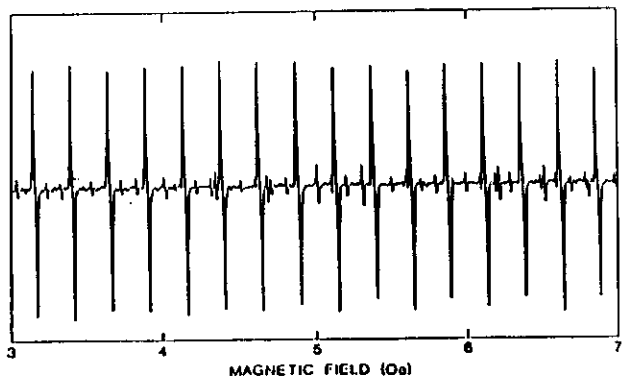Fig. 4. Modulated microwave absorption of YBa$_2$Cu$_3$O$_{7-\delta}$ single crystal at 4.4 K showing the regular absorption line series due to a naturally occurring SQUID structure in the crystal. The incident microwave power is 3 μW and the modulation amplitude 10 mOe.

Fig. 3. Modulated microwave absorption of a YBa$_2$Cu$_3$O$_{7-\delta}$ single crystal at 4.3 K between 38.5 and 41.5 Gauss. The incident microwave was 0.1 μW and the modulation field 5 mG. The external field is parallel to a ⟨110⟩ direction.
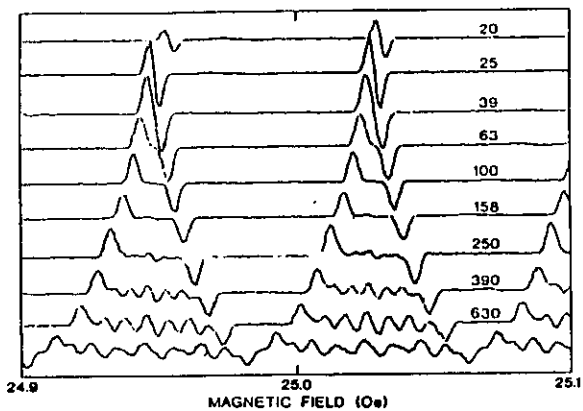
Fig. 5. Modulated microwave absorption of a YBa$_2$Cu$_3$O$_{7-\delta}$ single crystal at 4.4 K with 5 mOe modulation and the incident microwave power in μW indicated on each spectrum.

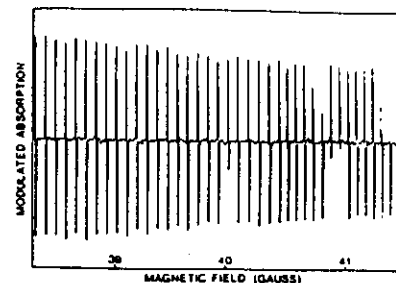$$H \cos \phi = \pm(p + \tfrac{1}{2})\Delta H$$

$$S = t(w + 2\lambda_L) = \phi_0/\Delta H$$

$$\lambda_L(T) = \lambda_L(0)[2(1 - T/T_c)]^{-1/2}$$

$$\lambda_L(T) = \lambda_L(0)[1 - (T/T_c)^4]^{-1/2}$$

K. W. Blazey, NATO Workshop, Crete (1989)

$$H_1 = H_{c1J} + 2\delta H$$

$$H_{c1J}(T) \approx \frac{4\pi}{c} \lambda_J(T) J_c(T)$$

where

$$\lambda_J = \frac{(\phi_0/4\pi)^{1/2}}{[4\pi/c\lambda_L J_c]^{1/2}}$$

$$J_c(T) \approx H_{c1J}(T)^2 \lambda_L(T)$$

$$H_{c1J}(T) \sim (1 - T/T_c)^{1.9 \pm 0.3}$$

$$J_c(T) \sim (1 - T/T_c)^{3.4 \pm 0.6}$$
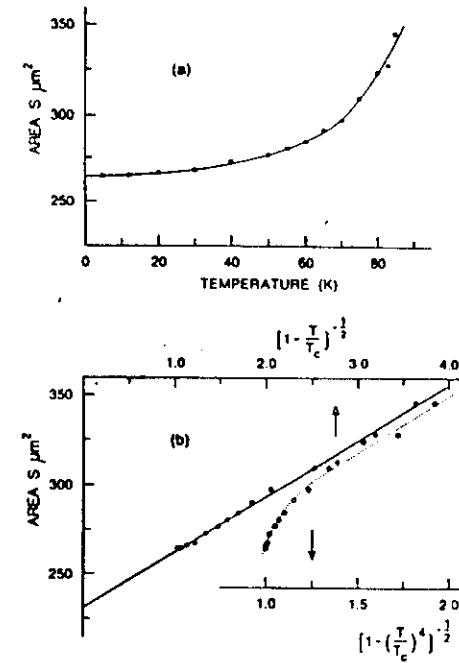
Fig. 4. (a) Temperature variation of the Josephson junction cross section $S = \phi_0/\Delta H$, responsible for the line absorption spectrum of Fig. 3. (b) The same temperature dependence assuming two different variations of the London penetration depth contribution to the cross section, S.
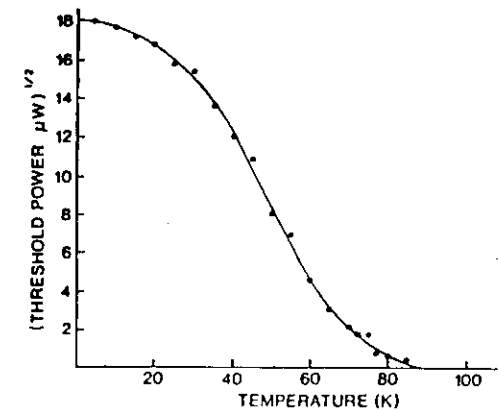

Fig. 5. The temperature dependence of the square root of the microwave threshold power required to generate the line spectrum of Fig. 3 at 5 Gauss.
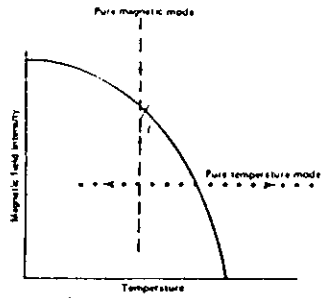
FIG. 1. Phase diagram for a superconductor showing pure temperature and pure magnetic mode paths for an EMR spectrometer.

sponding reflected microwave power spectrum and EMR response are similar to that shown in Fig. 2 but with H and T interchanged. Any other path can be taken by a combination of these two modes of operation.

There are two significant problems in implementing an EMR spectrometer to operate as described above. (1) It would be difficult to modulate the temperature, particularly at frequencies (10–100 kHz) normally used in ESR homodyne spectrometers. (2) For the type II superconductors which are of great current interest, the high critical field is beyond the range of conventional ESR magnets for all but a limited range of temperatures. Thus, an EMR spectrometer cannot be easily operated in either a pure temperature or pure field mode.

It is possible to operate in a hybrid mode which is a mixture of the pure temperature and field modes using tech-
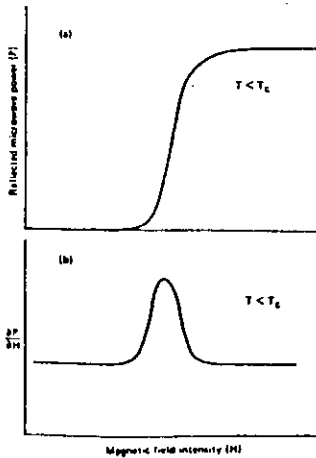

FIG. 2. Reflected power from a microwave cavity containing a superconductor at temperature $T < T_c$ as a function of magnetic field. (a) No field modulation or phase detection. (b) With field modulation and phase detection.

niques of conventional ESR spectroscopy. In this mode, a constant field ($H < Hc$) is imposed on the sample and the temperature is scanned as in the pure temperature mode, but the field is modulated instead of the temperature. The signal recorded at any temperature is (apart from a constant factor)

$$S = \left(\frac{\partial P}{\partial H}\right)_T \delta H. \tag{3}$$

It can readily be seen from Fig. 3 that

$$\Delta P = P(H + \delta H, T) - P(H, T)$$

$$= \left(\frac{\partial P}{\partial H}\right)_T \delta H = P(H, T + \delta T) - P(H, T)$$

$$= \left(\frac{\partial P}{\partial T}\right)_H \delta T \tag{4}$$

or

$$\left(\frac{\partial P}{\partial H}\right)_T \delta H = \left(\frac{\partial P}{\partial T}\right)_H \delta T. \tag{5}$$

The value of δT which results for a given δH according to this expression is independent of H and T in the region of the transition. Therefore the field modulation is equivalent to a temperature modulation in the region of the phase transition, and the spectrum recorded is the same as that of an ideal EMR spectrometer operating in the pure temperature mode with temperature modulation amplitude δT. At the same time, this hybrid mode of operation circumvents the problems encountered with operation in a pure mode. A bias field of sufficient magnitude that the net bias plus modulating field never changes sign is required in order that the modulation produce a response in $P(H)$ which is of the same frequency as the modulation frequency. Of particular importance for the application of this technique to superconductivity, is the fact that a signal will be recorded only if the microwave response is magnetic field dependent (i.e., $(\partial P/\partial H)_T \neq 0$). Thus, abrupt changes in microwave resistivity which are spurious or due to non-field-dependent phenomena (e.g., insulator-metal phase changes) will not be recorded by this method.

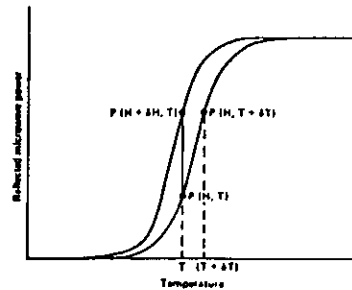The instrument used in this investigation is a home-built homodyne ESR spectrometer operating at X band (9.3

FIG. 3. Magnetic field dependence of reflected microwave power vs temperature for a superconductor.

GHz) with the microwave frequency locked to the cavity resonance frequency by a conventional automatic frequency control circuit. The microwave power incident on the samples was typically 2–200 mW (the maximum available with the microwave klystron used). The frequency of the modulating field was 10 kHz and its amplitude was typically 1–5 g. There were no indications of saturation effects or increased noise at the highest available microwave power and field modulation amplitudes, so there is at least some room to increase sensitivity by increasing these experimental variables. The sample temperature was controlled and varied using an Air Products LTD-3-110 Heli-Tran and model APD-E temperature controller.

RESULTS

In this section, we present some results on the use of this method to record superconducting transitions.

Figure 4 shows the microwave response by this technique for Nb, which is a well-characterized superconductor. The peak occurs at the transition temperature, and the width of the peak is a measure of the transition width. This spectrum was recorded with the magnetic field at 30 Oe.

A conventional microwave absorption spectrum of V_2O_3 powder, i.e., obtained by direct detection of the power reflected from the microwave cavity is shown in Fig. 5(a). This material exhibits an insulator-metal phase transition at approximately 150 K as evidenced by an abrupt change in the microwave absorption at that temperature. This phase transition is not magnetic field dependent, however, and therefore would not be recorded by the magnetically modulated microwave technique described here. Figure 5(b) shows the microwave response of this same sample using this technique. The absence of response to this phase transition illustrates the selectivity of our method for magnetic-field-dependent phase transitions.

Figure 6 shows the superconducting transition for two different samples of the perovskite, $YBa_2Cu_3O_{7-y}$ (YBCO). These samples each had an approximate mass of 1 mg. In Fig. 6(a), the results from a sample are shown in which two peaks are resolved. These peaks indicate the presence of two phases in the sample with slightly different critical temperature. The presence of these two peaks indicates
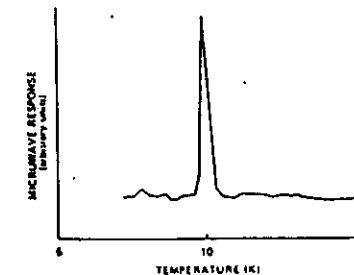

FIG. 4. Hybrid mode microwave response of an EMR spectrometer for Nb in the temperature region of the superconducting phase transition.
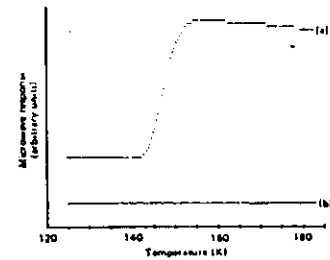

FIG. 5. (a) Conventional microwave absorption of V_2O_3 as a function of temperature. (b) Microwave response of the hybrid mode EMR spectrometer of V_2O_3 as a function of temperature.

an anomaly in the preparation of this particular sample. Figure 6(b) shows typical results for YBCO samples, in which a single peak is observed.

Figure 7 shows the results of a study in which the microwave loss spectra are recorded for a number of samples of YBCO (in powder form) each with known mass. These results indicate that the amplitude of the peak height scales directly with mass. This is an important result because it implies that this technique may be used to measure changes in the fraction of a sample which exhibits superconductivity. In this regard, we have used this technique to study the effects of high-energy ^{60}Co gamma radiation on the superconductivity of YBCO. These results will be described in detail elsewhere.

We have observed another aspect of this technique which provides additional information for the characterization of superconductors. This is illustrated in Fig. 8, which shows a temperature spectrum for a solid sample of YBCO in the temperature range 50–105 K. The onset of noise in the spectrum below the transition temperature, which increases with decreasing temperature, has been noted in many samples of this type. We have conjectured that this effect is caused by an ensemble of weak links or Josephson junctions between superconducting regions in the bulk samples. Results of a study of this phenomenon, which supports our conjecture, will be described elsewhere.
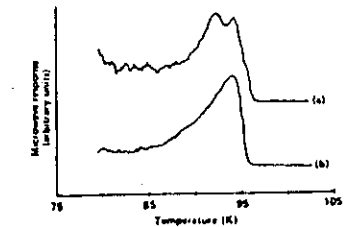

FIG. 6. Microwave response of $YBa_2Cu_3O_{7-y}$ in the region of the superconducting phase transition. (a) Sample containing two different superconducting phases. (b) Sample containing a single superconducting phase.

$BI_2 \ SR_2 \ CA_{N-1} \ CU_N \ O_X$ (N = 1, 2, 3 ...) IS A HIGH Tc SUPERCONDUCTOR

N = 2

$BI_2 \ SR_2 \ CA_1 \ CU_2 \ O_X$

c ≅ 31 Å

Tc ≅ 80 K

N = 3

$BI_2 \ SR_2 \ CA_2 \ CU_3 \ O_X$

c ≅ 37 Å

Tc ≅ 110 K

- Bi
- Sr
- Ca
- Cu
- O

$$\rho = \rho_0 + \frac{d\rho_0}{dT} \frac{dT_c}{dH} H_m \sin \omega_m t$$

$$H = H_0 + H_m \sin \omega_m t$$

$T_c (H_o + H_m)$ $T_c (H_o - H_m)$

$T_c (H_o)$

Temperature

Superconductor

$$\frac{dT_c}{dH} \neq 0$$

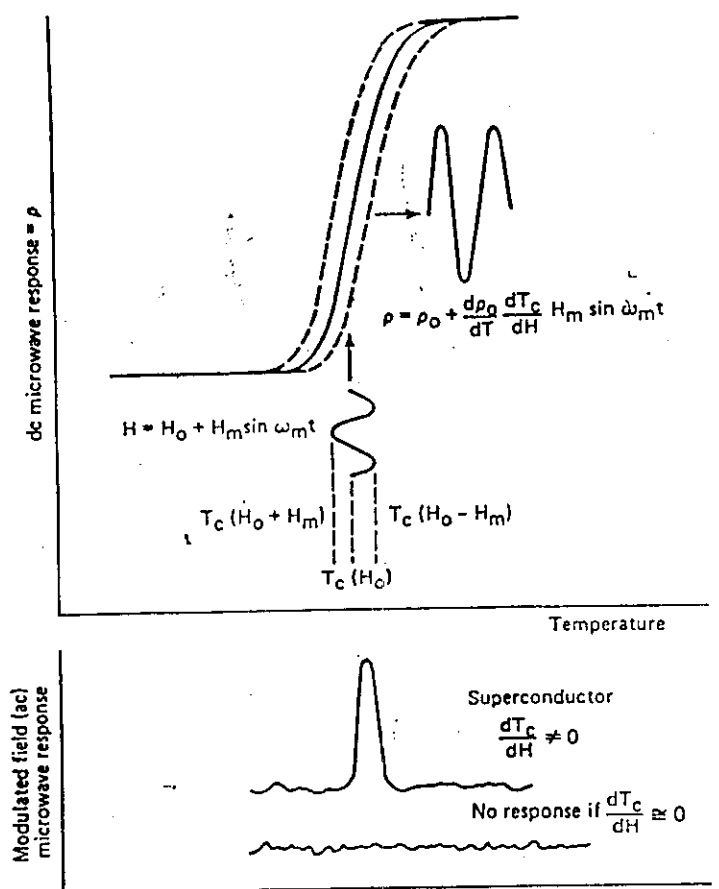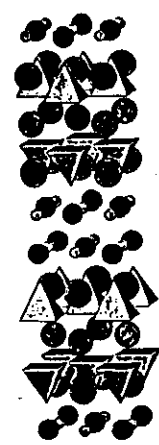No response if $\frac{dT_c}{dH} \cong 0$

Fig. 1   Schematic description of the magnetically-modulated microwave absorption for a superconductor ($dT_c/dH \neq 0$) and a field-independent ($dT_c/dH = 0$) transition.

K. Moorjani , B.F. Kim , J. Bohandy and F.J. Adrian ,

X - RAY DIFFRACTION

SAMPLE	STRUCTURE	C AXIS	
A - C	2212	31 A	(ENTIRELY)
D	2212	31 A	(HALF)
E	2223	37 A	(PREDOMINANTLY)
F - G	2223	37 A	(ENTIRELY)

(a) $Bi_2Sr_2CaCu_2O_z$;
(b) $Bi_2Sr_2Ca_2Cu_3O_z$;
(c) $Bi_2Sr_2Ca_3Cu_4O_z$;
(d) $Bi_2Pb_{0.4}Sr_2Ca_3Cu_4O_z$;
(e) $Bi_2Pb_{0.4}Sr_{2.2}Ca_{2.2}Cu_{3.3}O_z$;
(f) $Bi_2Pb_{0.4}Sr_2Ca_3Cu_4O_z$;
(g) $Bi_2Pb_{0.4}Sr_2Ca_4Cu_5O_z$.

G. Calestani, C. Rizzi, G.D. Andreetti, E. Buluggiu, D.C. Giorri, A. Valenti and G. Amoretti, Physica C 158 (1989) 217

G. Calestani et al., Physica C 158 (1989) 217

G. Calestani, M.G. Francesconi, G. Amoretti, C. Paracchini, E. Buluggiu, D.C. Giorri, A. Valenti and A. Vera, Physica C 162-164 (89) 526

The resistive absorption model

As discussed in [2], in the presence of a sufficiently low thermal activation energy, the phase-slip rate is so high that one sees its effect as a time-averaged dc-voltage. The effective resistance for $T \leq T_c$ may then be written

$$R = R_n[I_0(x)]^{-2}, \tag{1}$$

where

$$x = A(1 - t)^{3/2}/2H, \tag{2}$$

and I_0 is the modified Bessel function of order zero. R_n is the resistance in the normal state, $t = T/T_c$ the reduced temperature and H the external magnetic field. A is related to the value of the critical current density J_{c0} at $H = 0$ and in absence of thermal fluctuation effects (in the case of BSCCO, $A \simeq 3.75 J_{c0}$ with a in Oe and J_{c0} in A/cm^2).

Owing to the field-modulation typical of ESR technique, the revealed signal is proportional to the field-derivative of the microwave absorption P. Thus, we obtain [3]

$$\frac{\partial P}{\partial H} \propto \frac{(1 - t)^{3/2}}{H^2} \frac{I_1(x)}{I_0^3(x)}, \tag{3}$$

I_1 being the modified Bessel function of first order.

This expression can be more conveniently written in the two alternative forms

$$\frac{\partial P}{\partial H} \propto \frac{1}{H} F_1(x) \tag{4a}$$

$$\propto \frac{1}{(1 - t)^{3/2}} F_2(y), \tag{4b}$$

where $y = 1/x$ and we have defined the universal functions:

$$F_1(x) = x I_1(x)/I_0^3(x) \tag{5a}$$

and

$$F_2(y) = y^{-2} I_1(y^{-1})/I_0^3(y^{-1}). \tag{5b}$$

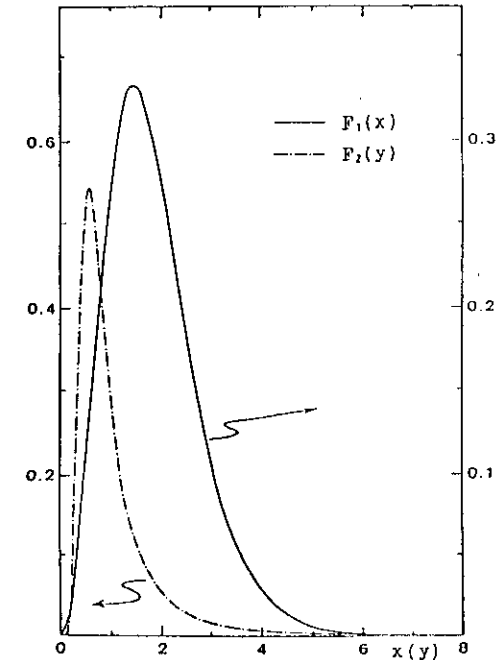The behaviours of $F_1(x)$ and $F_2(y)$ are shown in Fig. 3.

Fig. 3

[2] M. Tinkham, Phys. Rev. Lett. 61, 1658 (1988)

[3] E. Buluggiu, A. Vera and G. Amoretti, Physica C 171 (1990) 271

$$R_{powder} = \frac{1}{3} R_{\parallel} + \frac{2}{3} R_{\perp}, \tag{1}$$

or

$$R_{powder} = \frac{R_n}{2} \int_0^\pi \frac{\sin\theta}{[I_0(x(\theta))]^2} d\theta, \tag{2a}$$

where

$$x(\theta) = A(\theta)(1-t)^{3/2}/2H \tag{2b}$$

and

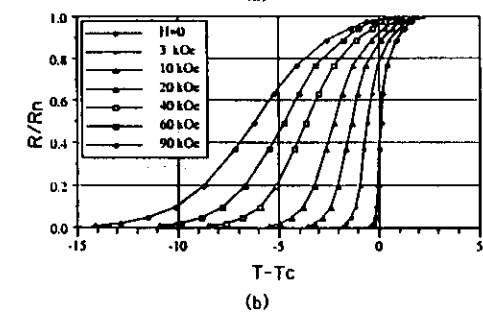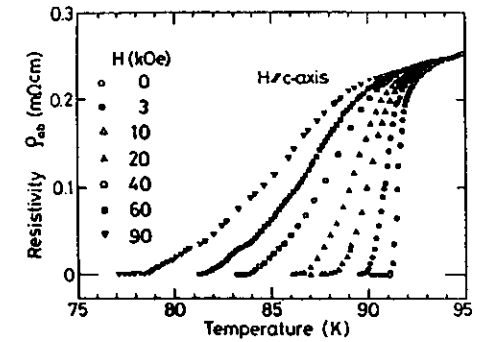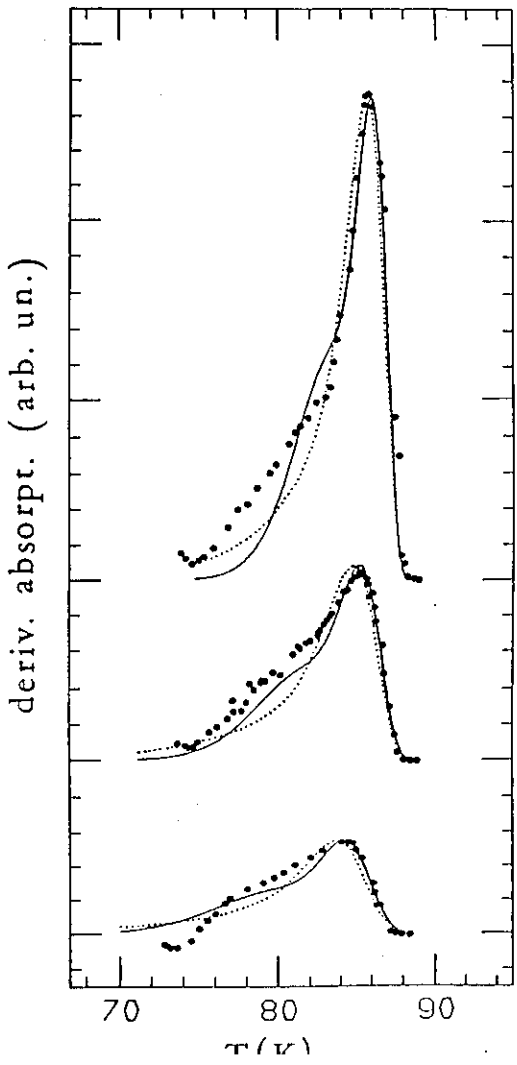$$A(\theta) = A_{\parallel} \cos^2\theta + A_{\perp} \sin^2\theta. \tag{2c}$$

(a)

(b)

FIG. 1. (a) $\rho_{ab}(T)$ of YBCO crystal for various values of H as reported in Ref. 6. (b) Computed curves from Eq. (6) with single fitting parameter A. At each level of R/R_n, the theoretical downshift $T_c - T$ is plotted relative to the *experimental* $R(T)$ curve for $H = 0$. No adjustment has been made for the general linear slope of $R_n(T)$.

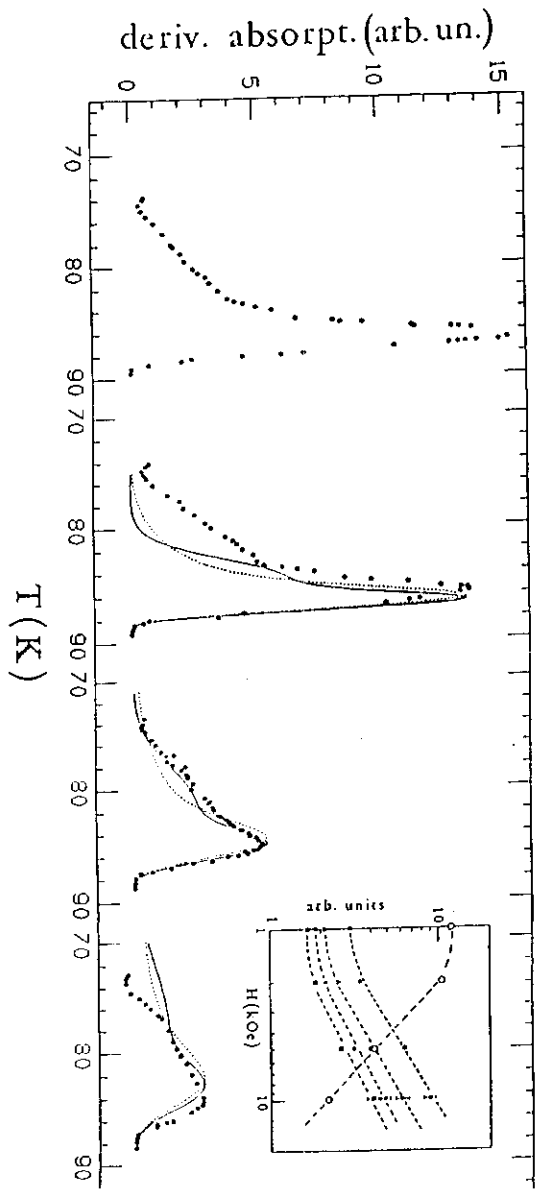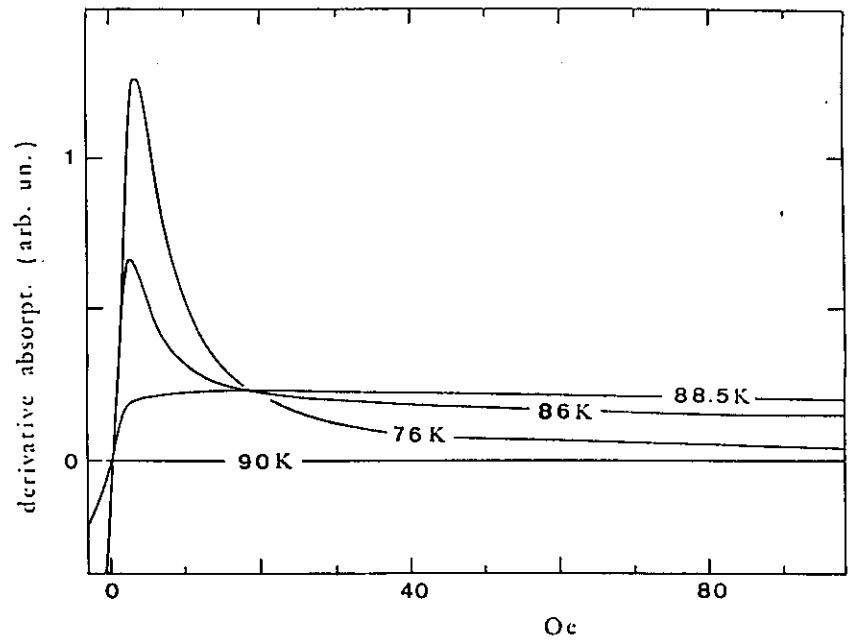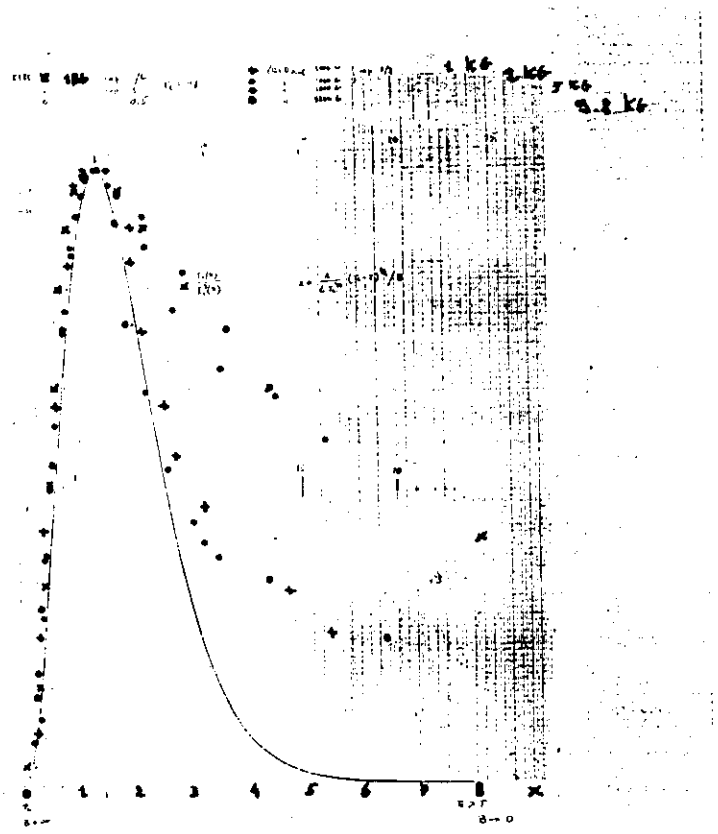M. Tinkham, Phys. Rev. Lett. **61**, 1658 (1988)

YBCO powder

Baleggio, Vera, Amoretti, Physica C 171 (1990) 271

deriv. absorpt. (arb. un.)

T(K)

arb. units

H(kOe)

Fig. 2

deriv. absorpt. (arb. un.)

YBCO powder

T(K)

YBCO powder

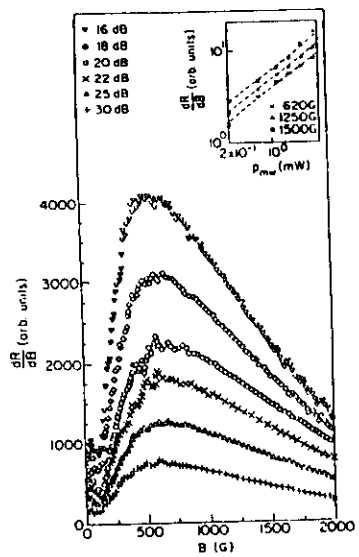E. Buluggiu, A. Vera and G. Amoretti, Physica C 171 (1990) 271

FIG. 1. Modulated microwave signal at various attenuations of full 200 mW for a Bi-Sr-Ca-Cu-O crystal at 76.5 K. The inset shows the dependence of the microwave signal on microwave power at three different fields on a log-log scale.
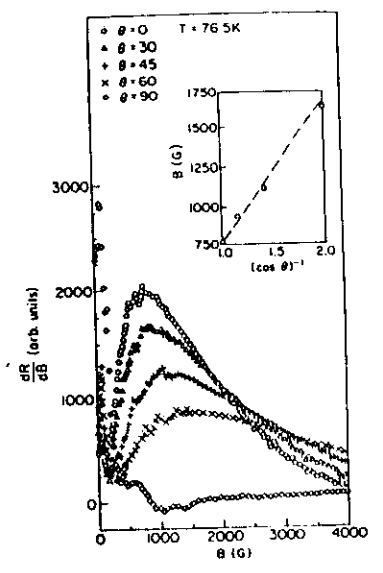

FIG. 2. Modulated microwave signals at different orientations: θ is defined by the angle between the dc field and the c axis of the same Bi-Sr-Ca-Cu-O crystal. The inset shows the peak field vs the $(\cos\theta)^{-1}$, and the dashed line is a guide for the eye.
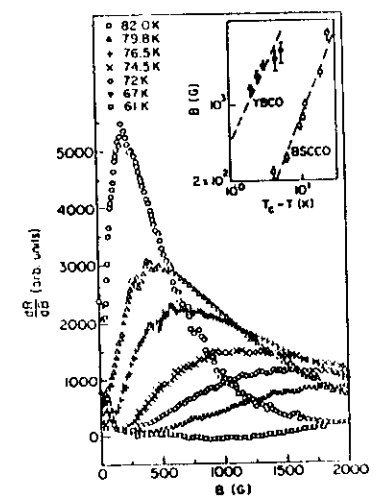

FIG. 3. Modulated microwave signal at various temperatures of a Bi-Sr-Ca-Cu-O crystal at $\theta = 0$. The inset is a log-log plot of the peak field value vs $(T_c - T)$ for both Bi-Sr-Ca-Cu-O and Y-Ba-Cu-O single crystals. The dashed lines are fits to the data.
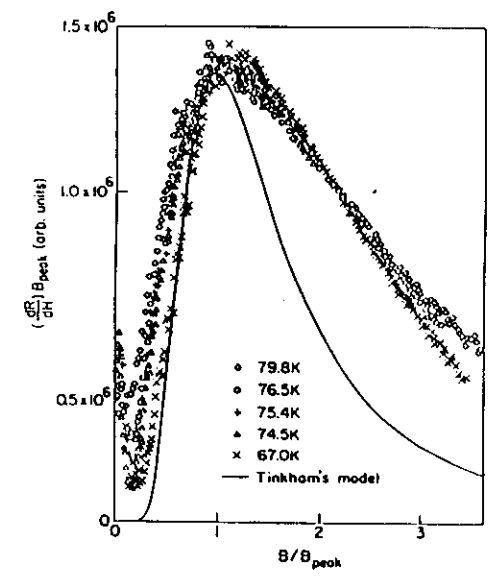

FIG. 4. Modulated microwave signal plotted with the x axis scaled to B/B_{peak} and the y axis scaled to $(dR/dB)B_{peak}$ at five different temperatures. The solid line is a fit with Tinkham's model.

BSCCO single crystal

Zuo et al., Phys. Rev. B 41, 6600 (1990)

$$\rho_h = \frac{2v_0 BL}{J} \exp\left[-\frac{U_0}{kT}\right] \sinh\left[\frac{JBV_cL}{kT}\right]$$

$$\rho_h = \frac{2v_0(BL)^2 V_c}{kT} \exp\left[\frac{U_0}{kT}\right]$$

$$U_0 = C(1-t)^{3/2}/B$$

$$\rho_f = \rho_n \frac{B}{B_{c2}}$$

$$\rho_t = \rho_n I_0^{-2}\left[\frac{A(1-t)^{3/2}}{2B}\right]$$

$$\rho_{expt} = F\left[\frac{B}{(1-t)^{3/2}}\right] \qquad \dot{Z} = R_n \frac{H}{H_{c2}} \frac{\omega(\omega+i\omega_0)}{(\omega^2+\omega_0^2)}$$

F. Zuo et al., Phys. Rev. B 41, 6600 (1990)

BSCCO : Pb   single crystal

$Bi_{1.7} Pb_{0.3} Sr_2 Ca Cu_2 O_8$ $T_c \simeq 86 K$

Fig. 1

G. Amoretti, D.C. Giori, E. Buluggiu, A. Vera,

From Fig. 1 it is evident that the temperature of the maximum T_M is strongly anisotropic, in line with the composite shape of the signal observed in powder samples. In particular

$$T_{M\perp} > T_{M\parallel}$$

with

$$\Delta T_M \simeq 4\ K \quad \text{at} \quad 2\ kOe$$

$$\Delta T_M \simeq 13\ K \quad \text{at} \quad 8\ kOe$$

T_M is decreasing with increasing field, in agreement with the relation

$$(1 - \frac{T_M}{T_c})^{3/2} = \frac{2.854}{A}\ H^\beta, \tag{6}$$

obtained on the basis of the Tinkham model for the magnetic field dependence of the resistivity.

We have found

$$\beta_\parallel \simeq 0.72 \quad \text{and} \quad \beta_\perp \simeq 0.36$$

to be compared with the theoretical $\beta = 1$ in the Tinkham model. This discrepancy was already observed in YBCO powders [3].

Following [2] with the theoretical value for β, we can estimate the zero-field critical current density J_{c0}. We obtain

$$J_{c0}^\perp \sim 2 \times 10^5 A/cm^2$$

and

$$J_{c0}^\perp / J_{c0}^\parallel \sim 3\text{-}5$$

in line with the assumption in ref. [3] for the powder resistivity

$$R_{powder} = \frac{1}{3}R_\parallel + \frac{2}{3}R_\perp. \tag{7}$$

As regards the intensity behaviour of the signal, it is seen that the height of the positive peak decreases as $H^{-0.9}$ in the parallel case, in substantial agreement with the theoretical H^{-1} dependence [3]. The decrease with increasing field is less strong in the perpendicular case.

As seen in Fig. 4, at fields lower than $\sim 100\ Oe$ the negative signal for $H \parallel c$ disappears, whilst the positive peak increases in height (at least up to 20 Oe). At these low fields a sort of "replica" of the signal appears at lower temperature, probably indicating the presence of lesser quality superconducting phases.

INTENSITY (arb. un.) vs **TEMPERATURE °K**

H par. c

o   0.02 kOe

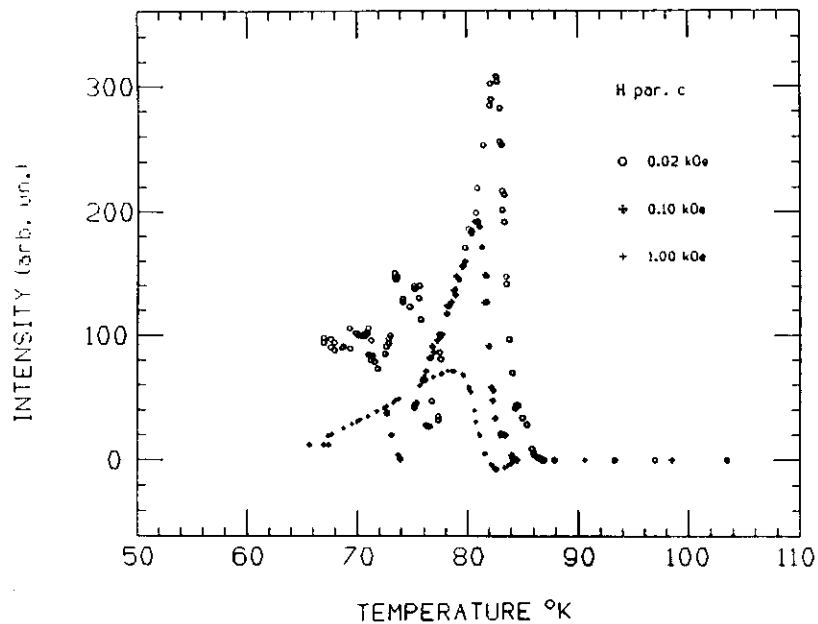+   0.10 kOe

+   1.00 kOe

Fig. 4
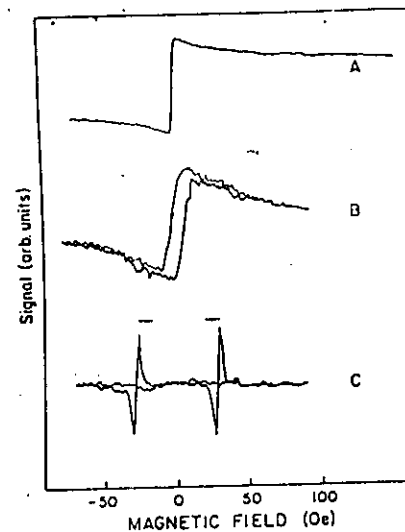
BSCCO : Pb   single crystal

FIG. 1. Representative microwave signals (phase detected at the fundamental of the field modulation) observed in well-oxygen-annealed single crystals of $YBa_2Cu_3O_x$ at temperatures (A) 86 K, (B) 64 K, (C) 36 K and $H_0\|c$.
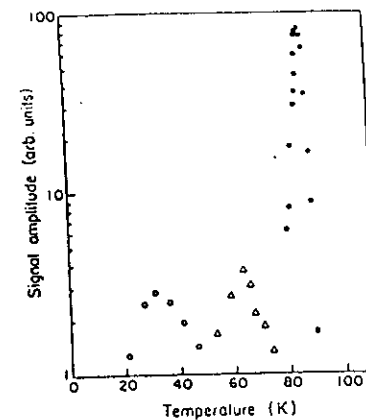

FIG. 2. Temperature dependence of the signals A (●), B (△), and C (○) (cf. Fig. 1) in a well-oxygen-annealed single crystal of $YBa_2Cu_3O_x$ for $H_0\|c$.
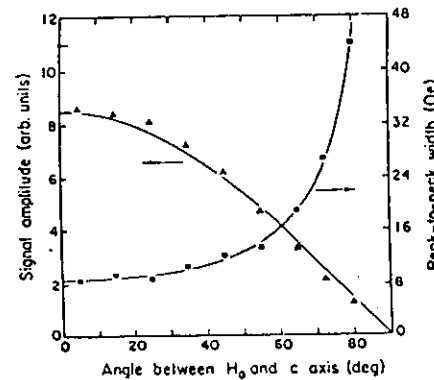

FIG. 3. Angular dependence of the peak-to-peak amplitude (▲) and width (■) of signal A (cf. Fig. 1).

A. Dulčić, R. H. Crepeau and J. H. Freed,
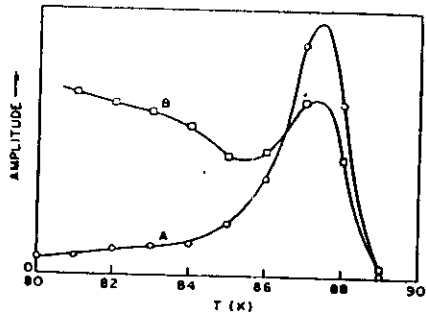
Phys. Rev. B 38, 5002 (1988)

FIG. 6. Temperature dependence of the step height for two single crystals. Crystal *A* has the lower impurity content.
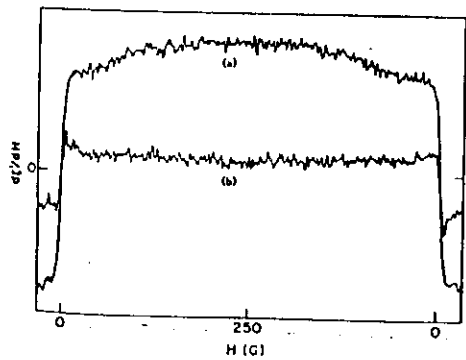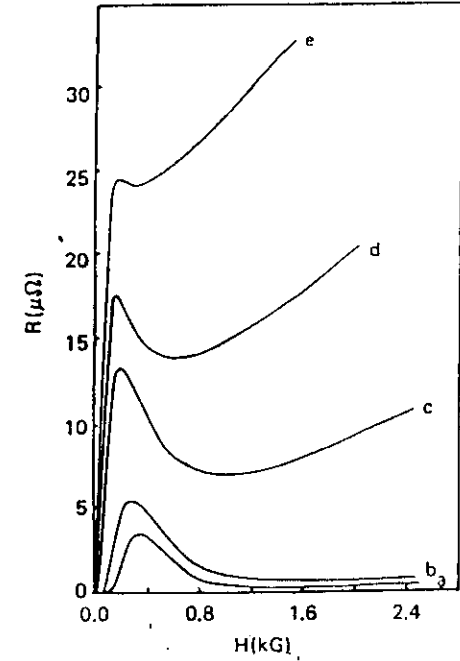

Fig. 1. The $R(H)$ characteristic of the sample at different temperatures, $I = 100$ mA, a: $T = 67.0$ K, b: $T = 70.7$ K, c: $T = 79.5$ K, d: $T = 85$ K, e: $T = 90.2$ K.
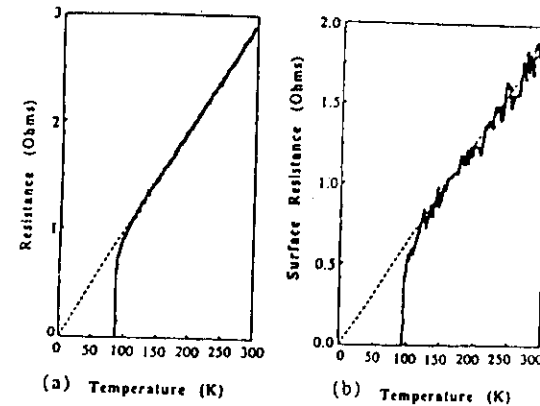
$Bi_{1.6}Pb_{0.4}Ca_2Sr_2Cu$

$T_c \sim 107$ K

FIG. 5. Derivative absorption spectra for a single crystal at 86 K with the *c* axis (a) parallel, and (b) perpendicular to the static field.

A. Inam et al., Appl. Phys. Lett. 56, 1178 (1990)

YBCO - film

(a) Temperature (K)   (b) Temperature (K)

FIG. 7 (a) +

S.H. Glarum et al., Phys. Rev. B 37, 7491 (1988)